Effect of the Distribution of Short-Chain Branches on Crystallization Kinetics and Mechanical Properties of High-Density Polyethylene

Rajendra K. Krishnaswamy* and Qing Yang

Chevron Phillips Chemical Company, LP, Bartlesville, Oklahoma 74004

Lucia Fernandez-Ballester and Julia A. Kornfield

Division of Chemistry and Chemical Engineering, California Institute of Technology, Pasadena, California 91125

Received February 21, 2007; Revised Manuscript Received October 26, 2007

ABSTRACT: The effects of the placement of short-chain branches (SCB) on crystallization kinetics, morphology and mechanical properties of high-density polyethylene (HDPE) are examined using bimodal blends of short (S ∼40 kg/mol) and long (L ∼400 kg/mol and 550 kg/mol) polyethylenes with SCB (1-hexene comonomer) incorporated in either the high or the low molecular weight component. A pair of blends that has nearly matched molecular weight distribution and average SCB content shows that placement of branches preferentially on the longer molecules results in slower crystallization kinetics at high crystallization temperatures relative to the material with branches on the short chains. Blends with SCB on the high molecular weight components have superior ultimate mechanical properties, and their resistance to slow crack growth is tremendously enhanced. These improved mechanical properties are attributed to an increase in the amount of tie chains that form when branches are placed on the long chains. A conceptual model based on the interplay of inherent crystallization kinetics of each species and their competition at the growth front in binary blends qualitatively explains the effects of SCB distribution on crystallization kinetics, lamellar thickness and inferred formation of tie chains.

Background

Over ten million metric tons of polyethylene (PE) are consumed in the USA every year.[1] The semicrystalline nature of polyethylene makes it a material of choice for many commodity and specialty applications. Crystallinity offers desirable attributes such as stiffness, strength, barrier to gas (e.g., moisture, oxygen) transport, chemical resistance, and dimensional stability. The noncrystalline phase imparts such attributes as toughness and resistance to slow crack growth. In many applications, the nature of the interlamellar noncrystalline phase is critical. For example, increasing the concentration of interlamellar tie-molecules enhances toughness and resistance to crack growth fracture.[2,3]

On a molecular level, an especially effective means to enhance the concentration of such tie-molecules is to incorporate noncrystallizable entities, such as short chain branches (SCB) from suitable comonomers such as 1-butene, 1-hexene, 1-octene, and 4-methylpentene-1, preferentially along the longest molecules of the polymer or blend.[2−4] Such a preferential placement of SCB is practiced commercially in many high-performance, high-density polyethylene (HDPE) applications.[4] Specific examples of such applications include high-strength packaging film and durable pipe for the transport of natural gas. One striking example that highlights the strength of PE can be found in the aftermath investigations of the Kobe (Japan) earthquake of 1995 during which the many fires and explosions from damaged gas pipelines caused considerable loss of life and property. However, none of the high-performance PE gas pipes failed even under this extreme service condition; it was the steel pipes that failed.[5]

The two types of SCB distributions that have been studied[6−24] incorporate SCB preferentially on the shorter chains or randomly distributed with respect to chain length, dictated largely by the polymerization catalyst used. Classical Ziegler−Natta ethylene copolymers have broad distributions of both molecular weight and SCB, with the greatest SCB on the shortest chains in the distribution. Metallocene-catalyzed copolymerization places SCBs relatively uniformly across the entire molecular weight distribution. In both cases, increasing SCB content systematically decreases the crystallinity, crystal growth rates and melting temperature. In addition, the interchain and intrachain heterogeneity of the branching distribution also influence the overall crystallization kinetics.[7−12,17] Generally speaking, for a given SCB content, crystallization of more random copolymers is slower than that of less random copolymers.

Table 1. Molecular Weight and SCB Characteristics of the Blend Components Used in This Investigation

component ID	M_w (kg/mol)	M_z (kg/mol)	M_w/M_n	SCB/1000 backbone carbon
L	398	823	2.9	0.0
L′	550	1110	2.6	0.0
L_b	389	782	2.9	5.6
S_b	35	54	1.9	4.7
S	45	242	5.3	0.0

Tensile properties of polymers are important in most applications. Therefore, the modulus at small deformations (E), the onset of nonrecoverable deformation (yield stress σ_y and strain ϵ_y) and failure (break stress σ_b and strain ϵ_b) have been extensively measured for unoriented polyethylene specimens of varying molecular weight and crystallinity levels.[10,11,25−36] For the classical Ziegler−Natta and the metallocene type SCB distributions, the small strain properties (E, σ_y, and ϵ_y) depend primarily on crystallinity (more specifically, lamellar thickness). Janzen and Register[26−28] observed that the self-consistent scheme derived by Hill and Budiansky[37,38] from continuum micromechanics described the increase of E and σ_y with density very well for PE. Further, ϵ_y decreased with increasing density. In summary, for the SCB distributions studied to date, the small-

* Corresponding author. Current affiliation: Metabolix, Inc., Lowell, MA 01854-3639. E-mail: krishnaswamy@telles-mirel.com.

10.1021/ma070454h CCC: $40.75
Published on Web 02/08/2008

Table 2. Molecular Weight Characteristics, Melt Rheological Attributes (CY Parameters) and Density after Identical Crystallization Conditions of the Binary Blends

blend ID	M_w (kg/mol)	M_z/M_w	M_w/M_n	η_0 (Pa·s)	τ_η (s)	a	av. SCB per 1000 BC	ρ (g/cm^3)
L/S$_b$-52/48	230	3.8	6.7	5.02E+04	0.36	0.57	2.3	0.9507
L/S$_b$-60/40	245	3.1	6.6	8.91E+04	0.45	0.57	1.9	0.9502
L/S$_b$-68/32	265	2.8	6.1	3.21E+05	1.32	0.39	1.5	0.9490
L$_b$/S-52/48	242	3.6	15.7	6.49E+04	0.39	0.54	2.9	0.9502
L$_b$/S-60/40	245	3.6	12.4	9.88E+04	0.46	0.56	3.4	0.9445
L$_b$/S-68/32	276	2.9	11.1	3.18E+05	1.21	0.41	3.8	0.9399
L′/S$_b$-52/48	276	4.4	11.9	1.51E+05	1.07	0.60	2.3	0.9485
L′/S$_b$-60/40	345	3.2	8.8	2.41E+05	1.30	0.62	1.9	0.9470

strain tensile properties of isotropic polyethylene depend only on density (or crystallinity)—not on molecular weight or spherulitic size.

In contrast to the small-strain deformation properties, the large strain tensile deformation properties of isotropic polyethylene, such as strain at break (ϵ_b) and tensile toughness, depend on the polymer molecular weight in addition to density.[25,30−34] For instance, higher molecular weight polymers are thought to increase the number of interlamellar tie-molecules, allowing the polymer to carry greater stresses and prevent it from deforming to high strains. Also, lower degrees of crystallinity allow for higher strain at break while carrying lower stresses. However, there are no reports to date that discuss the influence of SCB distribution profile on the ultimate tensile properties of PE.

A vast majority of failures in pressure pipe and geomembrane applications[39] occur at relatively low stresses and over long periods of time through the initiation and subsequent growth of a crack, typically referred to as slow crack growth or SCG.[39,40] This has led to the development of many lab-scale tests, such as the PENT (ASTM F1473) and the Full Notch Creep Test (FNCT; ISO 16770.3), that measure the resistance to SCG. The response of various polyethylenes to such lab-scale tests has been well documented.[2,3,41−56] Generally speaking, resistance to SCG improves with increasing molecular weight and with decreasing crystallinity (or density). It has been known since the early 1980s that SCB along the longest molecules of the molecular weight distribution are especially effective in enhancing resistance to SCG.[2−4,52−54]

Despite more than a decade of commercial practice using preferential placement of SCB along the longer molecules in HDPE (either through blending or the dual-reactor approach), very little is known about the crystallization characteristics of this type of SCB distribution. Further, commercial practice has been limited to Ziegler−Natta based PE components that contain a very heterogeneous distribution of SCB across their molecular weight distribution (MWD). In this study, we focus on bimodal blends based on relatively narrow-MWD components that have fairly homogeneous distribution of SCB across their MWD. By selectively blending homopolymers (linear PE) with copolymers, our study includes blends that are similar in their MWD and average SCB content, but differ in their SCB profile. We describe the effects of SCB distribution on quiescent crystallization kinetics, dynamic mechanical relaxation characteristics, tensile properties, impact toughness, and resistance to slow crack growth. We also present a schematic model that explains the observed effects of SCB placement.

Experimental Section

All of the component polyethylenes (Table 1) were synthesized in bench-scale polymerization reactors using a proprietary metallocene-based catalyst. The "long" chains include two samples that are essentially perfectly linear PE (L and L′ in Table 1) and one high-molecular weight copolymer of ethylene and a small amount of 1-hexene comonomer to provide 5.6 SCB/1000 backbone carbons (L$_b$ in Table 1). All three have relatively narrow MWD. The molecular weight and MWD of L$_b$ and L are very similar; they differ only in their SCB content. The low molecular weight blend components, "short chains", include one linear PE (S) and one ethylene-hexene copolymer containing 4.7 SCB/1000 backbone carbons (S$_b$). Nuclear magnetic resonance (NMR) was utilized to determine the SCB content in the copolymers using procedures described previously.[57] The SCB distribution in L$_b$ and S$_b$ was verified to be homogeneous using a sequential SEC−FTIR (size exclusion chromatography−fourier transform infrared spectroscopy) technique.[58] In other words, the average SCB content in the copolymers was verified to be constant across their MWD.

Pairs of long and short polymers were blended to create a series of materials with SCB on the "short" chains (L/S$_b$ and L′/S$_b$ blends) and a series with SCB on the "long" chains (L$_b$/S blends). The naming convention for the blends identifies which long chain species and short chain species are blended and the percentage of each. For instance, L/S$_b$-52/48 denotes the blend of 52% (by weight) of polymer L with 48% (by weight) of polymer S$_b$ (Table 2). Blending was done using a two-step procedure. First, calculated amounts of each component (nascent reactor powder) were weighed and the powder were mixed with suitable amounts of antioxidants (0.1 wt % Irganox 1010, a phenolic antioxidant from Ciba; 0.1 wt % P-EPQ, a high-activity phosphite from Clariant; and 0.05 wt % zinc stearate, an acid scavenger from Ferrell). This mixture was then tumble-blended to obtain a reasonably homogenized mixture. Subsequently, the tumbled mixture was extruded (at 200 °C) using a PRISM 16 mm 25:1 L/D co-rotating twin screw extruder; the extrudate strand was quenched in a water bath and pelletized.

The molar mass distribution and the SCB distribution of the blends (Table 2) were characterized using SEC (details in ref 57). The MWD of the blends did not show any appreciable deviation from what was anticipated based on the MWD of the components and the blend composition indicating minimal degradation during the melt-blending step. The M_w of the L/S$_b$ and L$_b$/S blend counterparts are similar; due to the greater length of L′ relative to L and L$_b$, the M_w of the "L′/S$_b$" blends are higher. The polydispersity of the blends are, for the sake of convenience, described in terms of M_z/M_w and M_w/M_n. The blends all have similar M_z/M_w. Because of the difference in the M_w/M_n between S and S$_b$, the M_w/M_n for the L$_b$/S blends is greater than that of the L/S$_b$ blends. The average SCB content, computed from the blend composition and SCB content of the individual components, is listed in Table 2. Of special significance is the pair of samples L/S$_b$-52/48 and L$_b$/S-52/48: these expose the effect of SCB distribution for roughly matched M_w, M_z/M_w, overall SCB content, and solid-state density. The other blends do not have matched counterparts; rather they reveal trends with increasing long chain content in cases when this coincides with decreasing SCB (L/S$_b$ and L′/S$_b$ blends) and in cases when this coincides with increasing SCB (L$_b$/S blends).

The melt rheology of the blends was characterized by performing dynamic oscillatory measurements at 190 °C. The resulting data ($|\eta^*|$ vs ω) were fitted to the Carreau−Yasuda (CY) eq 59:

$$|\eta^*| = \eta_0[1 + (\tau_\eta\omega)^a]^{n-1/a} \quad (1)$$

where $|\eta^*(\omega)|$ is the scalar magnitude of the complex viscosity, η_0 is the zero-shear viscosity, ω is the angular frequency, τ_η is the characteristic viscous relaxation time, a is a parameter that is inversely related to the breadth of the transition from Newtonian to power-law behavior, and n fixes the power-law exponent of the viscosity at high frequencies. In fitting the measured data to the CY model, n was assumed to be a constant (0.1818). The CY parameters (Table 2) show that the zero-shear viscosity trends are consistent with the trends in M_w. Consequently, the long-chain branching (LCB) content in these blends is surmised to be negligible; this was further verified using the Janzen-Colby semiempirical approach.[60] The melt rheological attributes of "L/S_b" and "L_b/S" blends are very similar.

All blends were compression molded by melting the pellets at 190 °C in a picture-frame mold, followed by slow-cooling. The refractive index of the molded slabs was measured using a Metricon 2010 prism coupling device. The density (one measure of crystallinity) of the blends was estimated from the refractive index values using the Lorentz−Lorenz equation, eq 61.

Quiescent crystallization experiments (isothermal and nonisothermal) were carried out under a nitrogen blanket using a Perkin-Elmer Diamond differential scanning calorimeter (DSC), which was calibrated using indium and zinc standards. Approximately 5−6 mg samples, in the form of circular disks, were used. For nonisothermal crystallization experiments, the specimens were first melted and equilibrated at 170 °C for 5 min after which they were cooled to 0 °C at rates ranging from 5 to 40 °C/min. The melting characteristics of the nonisothermally crystallized specimens were evaluated by subsequent heating from 0 to 170 °C at 20 °C/min. For isothermal crystallization experiments, a two-step cooling procedure was used: the specimens were equilibrated at 170 °C for 5 min, cooled first to 145 °C at 40 °C/min, held at 145 °C for 120 s, and then rapidly cooled (at 60 °C/min) to the desired isothermal crystallization temperature. With this procedure, the instrument transient concluded in less than 10 s; therefore, crystallization times as fast as $t_{peak} \sim 0.5$ min (t_{peak} is the time corresponding to the exotherm peak) could be measured. The specimens were maintained at the isothermal crystallization temperature for durations of up to 6 h. The melting characteristics of the isothermally crystallized specimens were evaluated by subsequent heating from the crystallization temperature to 170 °C at 20 °C/min.

Dynamic mechanical thermal analysis (DMTA) was employed to characterize the β and γ relaxations of the solidified blends (molded slabs) using a Seiko DMS200 instrument in the tension mode. Nonisothermal scans (in a nitrogen atmosphere) were performed between −140 and +120 °C at 1.5 °C/min; data were collected at 0.2, 1, 2, 10, and 20 Hz. Tensile stress−strain experiments were performed in accordance to ASTM D638 (dog-bone specimens that were 25.4 mm long, 6.4 mm in width and 2 mm in thickness). The crosshead speed was 51 mm/min. Five specimens were tested for each blend and the average numbers are reported. Razor-notched Charpy impact toughness tests were performed as specified by ASTM F2231, and PENT failure times (slow crack growth resistance) were measured according to ASTM F1473.

Results

To elucidate the specific impact of SCB placement on crystallization and melting behavior as well as on mechanical properties, we compare two blends with matched average molecular weight, MWD, and average SCB contents. The pair of blends L/S_b-52/48 and L_b/S-52/48 represent such a match: they have very similar M_w, MWD, rheological attributes, average SCB content, and similar density for slow-cooled specimens (Table 2). The main difference between L/S_b-52/48 and L_b/S-52/48 is in the distribution of SCB; therefore, their comparison will allow us to directly explore the influence exerted by preferential placement of SCB on either the long or the short chains. In addition, examination of the L′/S_b series as well as of other compositions for the L/S_b and L_b/S series will allow us to compare the trends on the crystallization and mechanical properties for blends with SCBs placed either on the high or on the low molecular weight component.

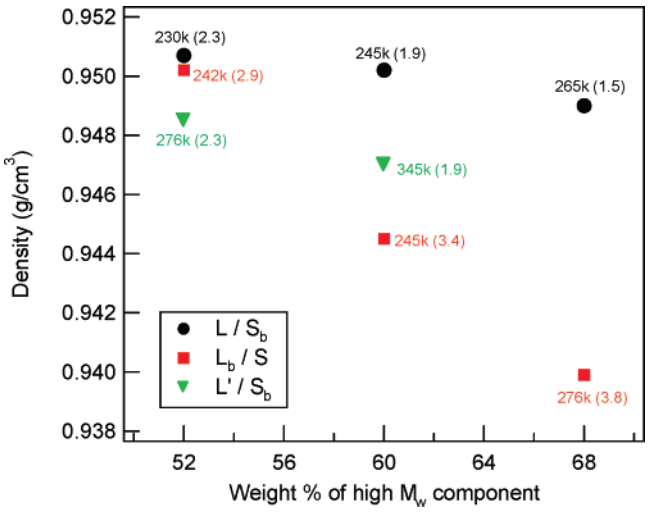

Figure 1. Density of slow-cooled blend specimens plotted as a function of blend composition. Next to each data point, the M_w (g/mol) and the average SCB content (within parenthesis, as SCB/1000 BC) are indicated. Note that the density of all blends falls within the range of high-density polyethylene.

Density and Microstructure of Slow Cooled Specimens. The density of compression-molded plaques of L/S_b-52/48 and L_b/S-52/48 are very similar (Figure 1): the placement of the SCB on the high or on the low molecular weight component for materials with matched M_w, MWD, shear rheology and average SCB content does not affect the overall level of crystallinity. An increase in molecular weight (all else being equal) results in lower crystallinity (compare each L′/S_b blend to its L/S_b counterpart). This effect is offset when SCBs are placed on the short chains, because SCB content decreases while M_w increases. Conversely, for L_b/S blends, the crystallinity decreases substantially with increasing amounts of the high molecular weight component due to the combined effect of increasing molecular weight and increasing SCB content. For all these compression-molded specimens, the density results (Figure 2) accord well with heat of fusion results.

The spherullitic morphology in slow cooled specimens show differences that suggest SCB distribution affects the relative rates of growth and nucleation. Small angle light scattering patterns (H_v SALS in Figure 2) all show the four lobe pattern characteristic of spherullitic super-structure. On the basis of the two blends that have very nearly matched M_w, overall SCB content and degree of crystallinity (based on density and heat of fusion), placement of SCB preferentially on the long chains decreases spherullite size: the peak intensity occurs at a slightly larger angle for L_b/S-52/48 than for L/S_b-52/48. A decrease in spherullite size occurs when the growth velocity slows relative to the nucleation rate. Thus, it appears that for fixed overall SCB content, placing them on the long chains retards propagation of crystals (more so than nucleation). Increasing long chain content affects morphology differently when accompanied by a reduction in SCB (L/S_b-60/40) than by an increase in SCB (L_b/S-60/40). For blends in which M_w is increased while decreasing SCB, the spherulites become more uniform in size and shape: the four-lobe pattern is well-defined for L/S_b-60/40, rather than diffuse for L/S_b-52/48. On the other hand, increasing both M_w and SCB results in smaller, more irregular

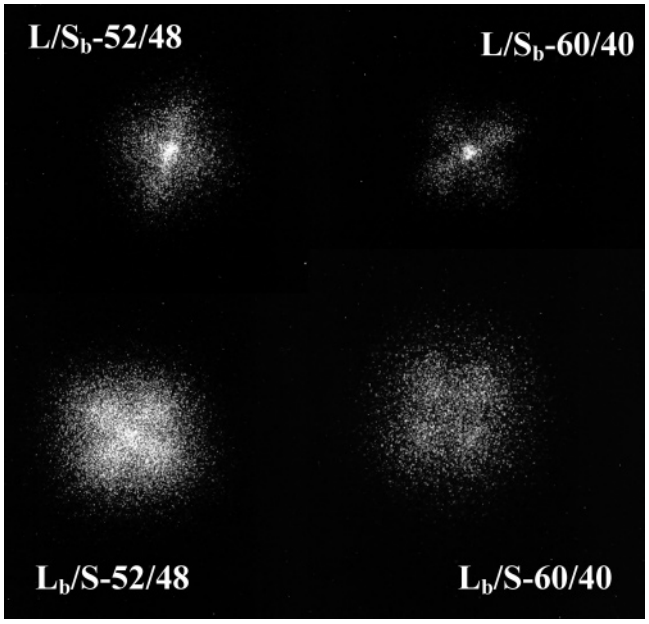

Figure 2. SALS patterns of representative slow-cooled blend specimens showing the four-leaf clover pattern.

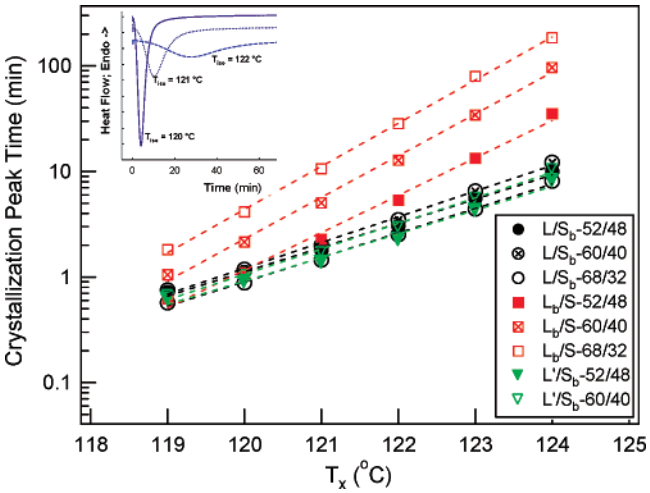

Figure 3. Peak location of the isothermal melt-crystallization exotherms, t_{peak}, plotted as a function of crystallization temperature for all blends. The inset shows representative isothermal crystallization exotherms for L_b/S-52/48 at three temperatures. The exotherms become broader and their location shifts to longer times at higher crystallization temperatures T_x; also, the enthalpy of crystallization decreases slightly with increasing temperature, as expected.

spherullites: the lobes in the SALS pattern of L_b/S-60/40 are more diffuse and extend to greater angle than those of L/S_b-52/48. Note that the shifts in peak position are mild in all cases, indicating that the nucleation density is similar.

Isothermal Crystallization Kinetics. The most striking effect of SCB placement on isothermal crystallization kinetics (Figure 3) is pronounced slowing that occurs when the effect of SCB content and M_w reinforce each other: across the L_b/S blends, the crystallization time increases substantially with simultaneously increasing long chain content and SCBs. A subtle, but interesting, feature is the virtual absence of any effect of changing chain length at fixed SCB content when branches are on the short chains (compare L/S_b and L′/S_b analogues). Similarly, the absence of an effect of blend ratio on crystallization time for the L/S_b blends is noteworthy.

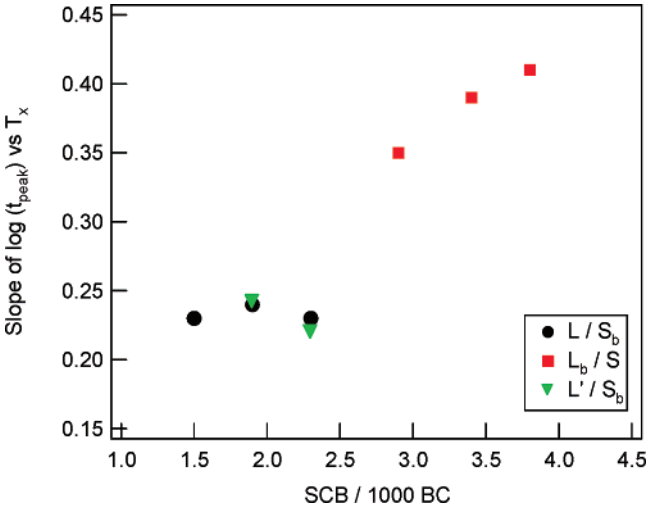

Figure 4. Slope extracted from Figure 3 (log(t_{peak}) vs crystallization temperature) plotted as a function of total SCB content in the blends.

At low undercoolings (high T_x), the blends with SCB on the longer molecules are significantly slower to crystallize, while at high undercoolings, the crystallization time scales for the various blends tend to converge. For example, despite the similar molecular weight, MWD, shear rheology, and average SCB content for blends L/S_b-52/48 and L_b/S-52/48, the crystallization kinetics of L_b/S-52/48 are substantially slower at high T_x, and become similar as crystallization is performed at progressively lower temperatures. In other words, preferential placement of SCB on the longer molecules makes them more sluggish (from a crystallization perspective) at low undercoolings.

As is often observed, t_{peak} increases approximately exponentially with increasing T_x. As can be seen in Figure 3, the slope of log t_{peak} vs T_x is lower for the "L/S_b" and "L'/S_b" blends than for the "L_b/S" blends (Figure 4). For "L/S_b" and "L′/S_b" blends, the slope does not appear to depend on SCB content: the effect of increasing molecular weight appears to be offset by decreasing SCB content. For "L_b/S" blends, this slope is much larger and it increases with SCB content. A separation of the two data sets is evident: clearly the crystallization kinetics of PE are not only a function of average SCB content, but that they also depend on how the SCB is incorporated across the MWD of the polymer. With little difference previously noted in the nucleation density of these blends, these findings suggest that preferential placement of SCB along the longer molecules makes lamellar growth more sluggish particularly at low undercoolings than placement of SCB along the shorter molecules.

The above isothermally crystallized specimens were subsequently heated from the isothermal temperature to observe the melting transition. The peak melting point (T_m) decreases with increasing molecular weight for the L_b/S blends, which can be explained in terms of higher SCB content (Figure 5). In contrast, the L/S_b blends (L/S_b-60/40, and L/S_b-68/32) show no discernible effects of increasing long-chain content. Preferential placement of SCBs on the short chains makes the blends insensitive to the average SCB content and to the average length of the long (unbranched) chains.

The usual systematic increase in T_m with increasing crystallization temperature is clearly evident (Figure 5). Thicker and more perfect lamellar crystals are formed at higher temperatures (lower undercooling). The increase of T_m with T_x is steady for blends with branches on the short chains; however, for blends

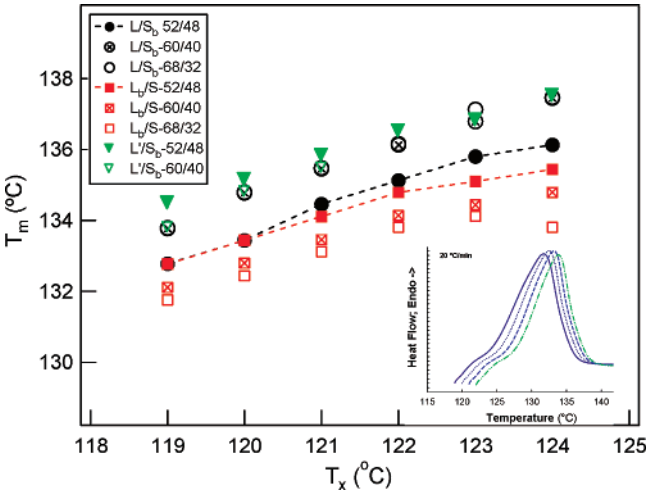

Figure 5. Peak melting point plotted as a function of isothermal crystallization temperature for all blends. The inset shows the melting endotherms for representative, isothermally crystallized L_b/S-52/48 specimens (the starting points of the endotherms indicate the isothermal crystallization temperature).

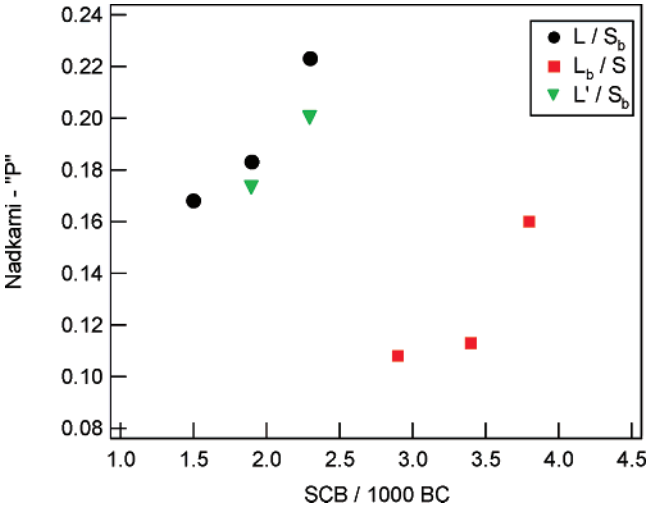

Figure 6. Nadkarni "*P*" parameter (from nonisothermal melt-crystallization experiments) plotted as a function of total SCB content in the blends.

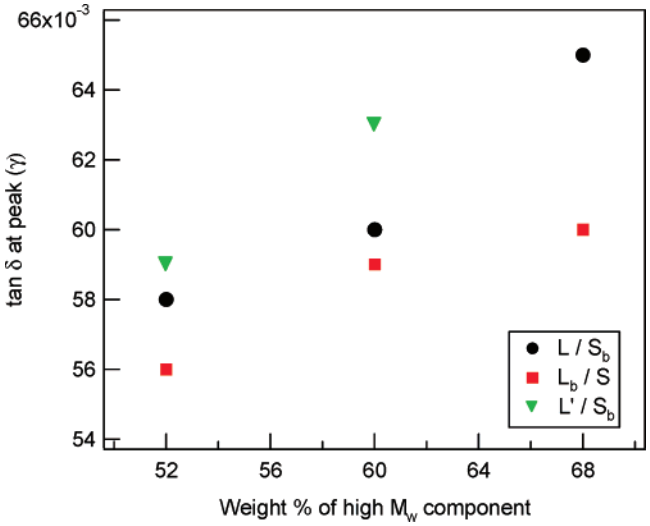

Figure 7. tan δ magnitude at the γ relaxation peak location (at 10 Hz), plotted as a function of blend composition.

with SCB on the long chains, T_m reaches a plateau or even decreases at the upper range of T_x. For L_b/S blends, the anticipated increase in T_m with molecular weight is countered by the decrease in T_m with increasing SCB. The subtle change in slope at about $T_x \sim 122$ °C, observed for all blends, may be attributable to a Regime-III to Regime-II transition in crystallization behavior.

Nonisothermal Crystallization Kinetics. Empirical equations can be used to extract quantitative characteristics from the nonisothermal exotherms.[62−64] Nadkarni's approach[63] analyzes nonisothermal crystallization data in terms of the degree of undercooling ΔT_c, defined as the temperature difference between the temperature at the onset of crystallization T_b, and T_m in the subsequent heating scan. The variation of ΔT_c with cooling rate, χ, is fitted to the following equation:

$$\Delta T_c = P\chi + \Delta T_c^{\,0} \qquad (2)$$

where $\Delta T_c^{\,0}$ is the degree of undercooling required in the limit of zero cooling rate and thought to be related to the thermodynamic driving force for nucleation, and the slope, P, is a process sensitivity factor that accounts for the kinetic effects.

For all of the samples, $\Delta T_c^{\,0}$ was 15 ± 1 °C, indicating that their nucleation densities are similar, in accord with the similar spherulite sizes evident in the light scattering patterns discussed above (Figure 2). In contrast, the sensitivity to cooling rate, P, was substantially affected by SCB distribution (Figure 6). A clear trend of increasing P with increasing SCB content is evident for all blends. However, P is significantly smaller for "L_b/S" blends relative to "L/S_b" and "L′/S_b" series, which indicates that the blends with SCB preferentially located along the longer molecules have a crystallization rate that is less sensitive to cooling rate. These results qualitatively accord with the differences seen in isothermal crystallization.

Dynamic Mechanical Relaxation Characteristics. Solid-state dynamics were very similar for all the blends, consistent with all of them having sufficiently high density to be considered HDPEs. The dynamic relaxation characteristics of the blends show the three distinct relaxations characteristic of PE.[65−70] With increasing temperature, the storage modulus decreases and the loss modulus shows three peaks. These are ascribed to: short range segmental motions in the noncrystalline regions (sometimes envisioned as relaxation of segments comprising four methylene groups) that are activated at approximately −100 °C (γ relaxation); the glass transition of polyethylene below −10 °C (β relaxation); and motion of chains within the crystalline phase and the adjacent "interphase" regions that increase strongly with temperature above 50 °C (α relaxation).

First, the strength of the γ relaxation, as indicated by tan δ at the γ peak (Figure 7) is *not* a good indicator of the fraction of noncrystalline phase in PE. The lowest and highest values of tan δ were observed for samples having very similar density (Figure 1, L_b/S-52/48 and L/S_b-68/32). This contradicts previous assertions that the γ relaxation strength is directly correlated to density.[66−69] Across the L/S_b series, tan δ increases substantially despite the fact that the density is nearly constant. Therefore, although the increase in tan δ across the L_b/S series might be attributed to the increase in noncrystalline fraction, a full interpretation should also consider the local chain structure in the noncrystalline regions. The trend across the L/S_b series suggest that, although the amount of noncrystalline material is roughly constant, the increase in the fraction of unbranched PE in these regions dominates to produce an increase in the strength

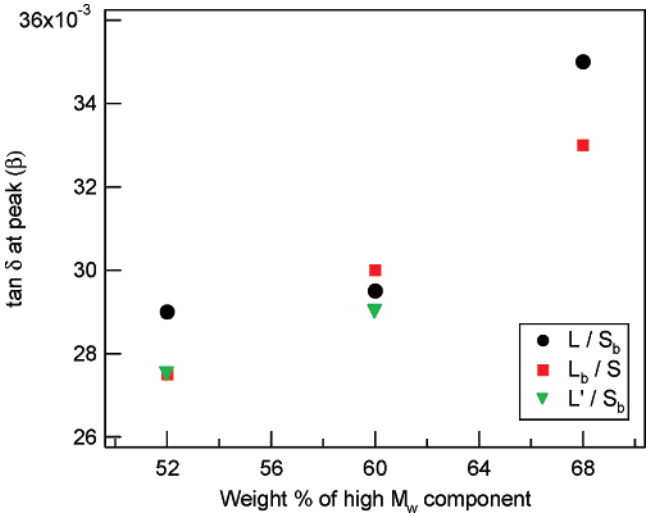

Figure 8. Magnitude of tan δ at the β relaxation peak location (at 10 Hz), plotted as a function of blend composition.

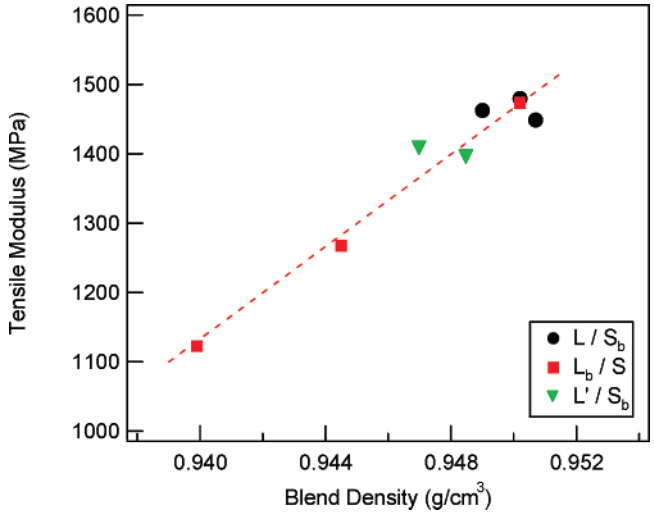

Figure 9. Tensile modulus plotted as a function of density for all the blends.

of the γ transition. Conversely, the trend across the L_b/S series show a weaker increase in the γ relaxation despite a much greater increase in noncrystalline fraction; the high fraction of SCB on the chains in the noncrystalline regions causes the γ transition to be much weaker than one would expect based on density alone.

The second trend that is *not* seen is an increase in the β relaxation strength with increase in the noncrystalline fraction, contrary to previous reports.[66−69] Again the lowest and highest values of tan δ, here for the β relaxation, are observed for samples of similar density (Figure 8, L_b/S-52/48 and L/S_b-68/32). And, again, across the L/S_b series there is a substantial increase in the β relaxation even though the density is nearly constant. Neither the location nor the strength of the β transition correlated with crystalline fraction or SCB content. As with the γ relaxation, there is a coupled effect of the amount of noncrystalline material and the molecular structure of the chains that are in it.

Mechanical Properties: Tensile. The instantaneous tensile properties, namely modulus (E), yield stress (σ_y), and yield strain (ϵ_y) were found to depend exclusively on density (or crystallinity), as expected (Figure 9): the modulus increases systematically with increasing crystallinity irrespective of SCB distribution or M_w. The yield stress and strain showed similar correlations with density, with σ_y increasing and ϵ_y decreasing with increasing crystallinity.

In contrast, blends with the same density can have pronounced differences in their ultimate properties—the stress and strain at which they fail (Figure 10). For example, L/S_b-52/48 and L_b/S-52/48 are similar in M_w, SCB content, density and E, yet L_b/S-52/48 has substantially (25%) greater break stress and lower strain at break than L/S_b-52/48. Preferential location of SCB along the longer molecules increases the tie-molecule concentration sufficiently that the semicrystalline structure is able to sustain substantially higher levels of stress prior to breakage. In other words, placing a few SCB on the longest molecules of a PE produces the tensile traits of a significantly higher molecular weight polymer, all else being equal.

It is striking that each of these ultimate properties varies similarly with increasing long chain content across the L_b/S and L/S_b series of blends—despite the fact that the density hardly varies in the L/S_b series and decreases substantially across the L_b/S series. Initially, the break stress increases somewhat with

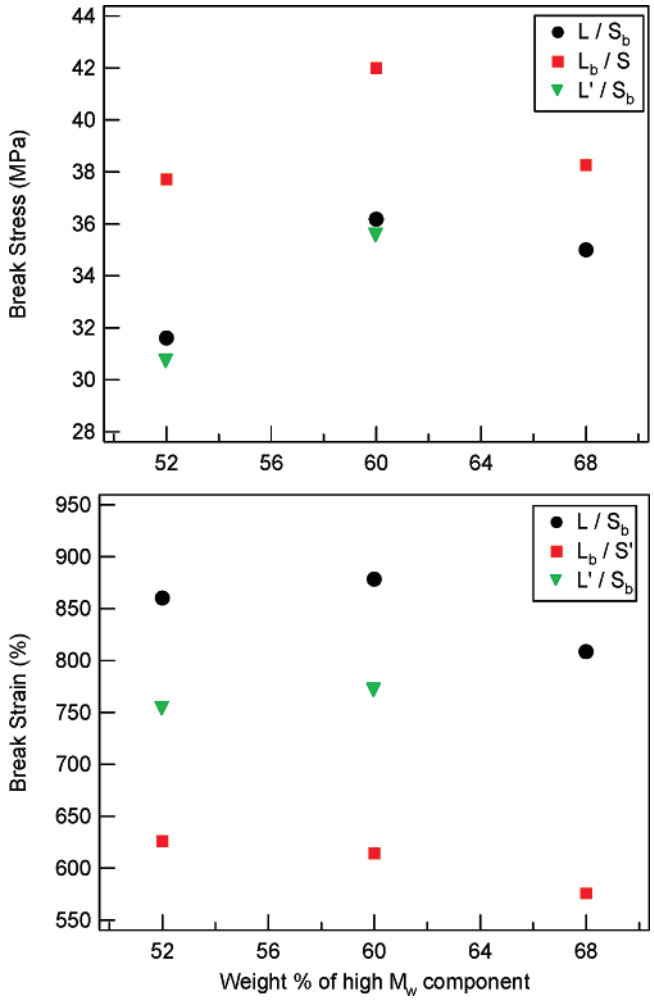

Figure 10. Tensile stress and strain at break plotted as a function of blend composition for all the subject blends.

molecular weight; however, at the highest molecular weight in each series, the break stress decreases. These maxima in the break stress vs blend composition partially reflect competing effects between molecular weight and crystallinity. Thus, the blends with SCB on the long chains consistently have greater break stress and lower break strain than L/S_b (and L′/S_b) blends.

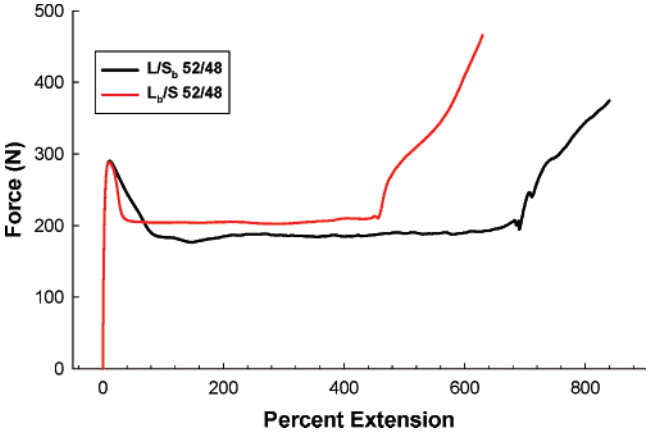

Figure 11. Representative tensile load-displacement curves for blends L/S$_b$-52/48 and L$_b$/S-52/48 highlighting the effect of SCB distribution on "strain-hardening" behavior.

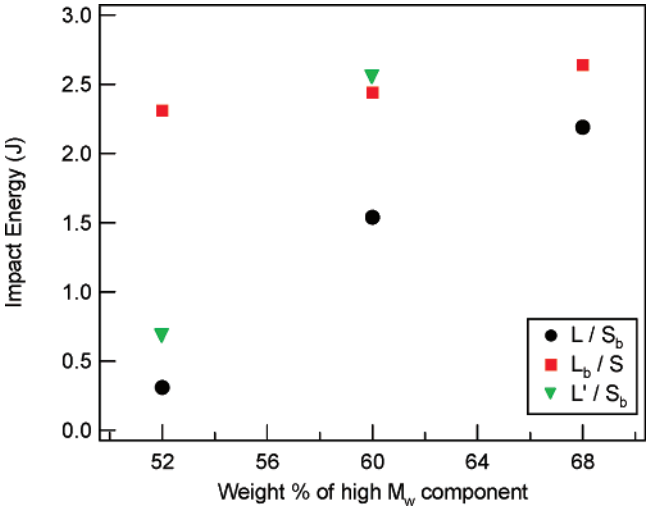

Figure 12. Charpy (razor-notched; ASTM F2231) impact energy (measured at room temperature) plotted as a function of blend composition for all the subject blends.

Despite the crystallinity and molecular weight differences between the three blend series, SCB distribution appears to exert the strongest influence on the ultimate tensile properties of PE.

The full tensile curves illustrate the features described so far and an additional important property: the natural draw ratio. In accord with the correlation between instantaneous properties (E, σ_y, and ϵ_y) and density, the raw tensile curves coincide at small strain for L/S$_b$-52/48 and L$_b$/S-52/48 (Figure 11). At failure, L$_b$/S-52/48 has greater stress and lower strain at break than L/S$_b$-52/48, in accord with the effect of SCB distribution noted above. Between the yield peak and failure, additional features are noteworthy: the plateau stress and the onset of strain hardening. As the nominal strain initially increases, the load increases to a maximum that coincides with the transition from homogeneous elongation to necking. As elongation continues, the neck becomes longer. The load required to propagate the neck is constant, leading to a broad plateau. Placement of SCB on the long molecules increases this plateau load: the energy required to propagate the neck in L$_b$/S-52/48 is greater than that for L/S$_b$-52/48. Once the neck encompasses the full length of the specimen, homogeneous elongation resumes and the load required to continue elongation increases sharply. The elongation at the onset of strain hardening, the "natural draw ratio", is much lower for L$_b$/S-52/48 than for L/S$_b$-52/48. Thus, the energy required to force the sample to yield beyond approximately 4-times its initial length is much greater for the L$_b$/S blend. The ability of "L$_b$/S" blends to sustain higher loads prior to failure is a consequence of this earlier onset of strain-hardening. Again, comparison of these two blends shows the effect of SCB placement holding M_w, SCB content, ρ, E, σ_y, and ϵ_y all nearly constant. The natural draw-ratio is thought to be a consequence of interlamellar tie-molecule concentration and is therefore considered to be a reasonable indicator of the long-term fracture behavior and durability of PE products.[71−76] This is the first report that describes the relationship between strain-hardening character of PE and SCB distribution.

Mechanical Properties: Impact Fracture and Slow Crack Growth. The razor-notched Charpy impact toughness (ASTM F2231) provides a reasonably good indication of the plane−stress fracture toughness of polyethylene specimens.[77,78] Within each blend series, the impact energy at 25 °C increases with increasing amounts of the high molecular weight component (Figure 12), as expected based on the usual improvement of the energy absorbing capacity of polymers with increasing molecular weight. It is striking, however, that this effect of chain length is almost completely offset by the decrease in density due to increased SCB content across the L$_b$/S series. In contrast, the effect of increasing M_w is strongly enhanced in the L/S$_b$ (and L′/S$_b$) series by the concomitant decrease in SCB content. Blends that place SCB on the long chains (e.g., L$_b$/S-52/48) provide access to impact toughness that requires substantially greater M_w to achieve with SCB preferentially on the short chains (e.g., L′/S$_b$-60/40). Closer examination of the data indicates that branching distribution exerts a strong influence, with preferential placement of branches along the high molecular weight component favoring toughness. For instance, while the MWD, shear rheology, and total branch content of L/S$_b$-52/48 and L$_b$/S-52/48 are very similar, the impact energy of L$_b$/S-52/48 is almost 10 times that of L/S$_b$-52/48. However, at sufficiently high molecular weights, the dependence on branching distribution appears to be somewhat diminished as the impact energies of blends L/S$_b$-68/32 and L$_b$/S-68/32 are quite similar.

All of the subject blends failed in a ductile manner when tested at room temperature. The impact energy is known to decrease with decreasing temperature; at temperatures below a critical value, the impact energy decreases rather abruptly to a low-temperature plateau with the failure mode becoming predominantly brittle. The temperature at which this ductile to brittle transition occurs is important in many applications such as gas transport pipes.[78] Specifically, this ductile-brittle transition temperature is thought to provide a good indication of the useful service temperature window for gas transport pipes in cold temperature environments.[78] For blends L/S$_b$-52/48 and L$_b$/S-52/48, the Charpy impact measurements were also carried out at multiple subambient temperatures down to −35 °C to determine the ductile to brittle transition temperature. This transition temperature was approximately −18 °C for L/S$_b$-52/48. For L$_b$/S-52/48, the fracture mode was ductile at all temperatures tested, suggesting the ductile−brittle transition occurs below −35 °C. This clearly shows that the low-temperature impact toughness of polyethylene is strongly dependent on branching distribution, with preferential placement of SCB along the longer molecules substantially expanding the service temperature range at low temperatures.

The PENT failure times for the various blends within each series show the familiar systematic improvement in SCG resistance with increasing molecular weight (Table 3). In the L/S$_b$ series, the beneficial effect of increasing molecular weight

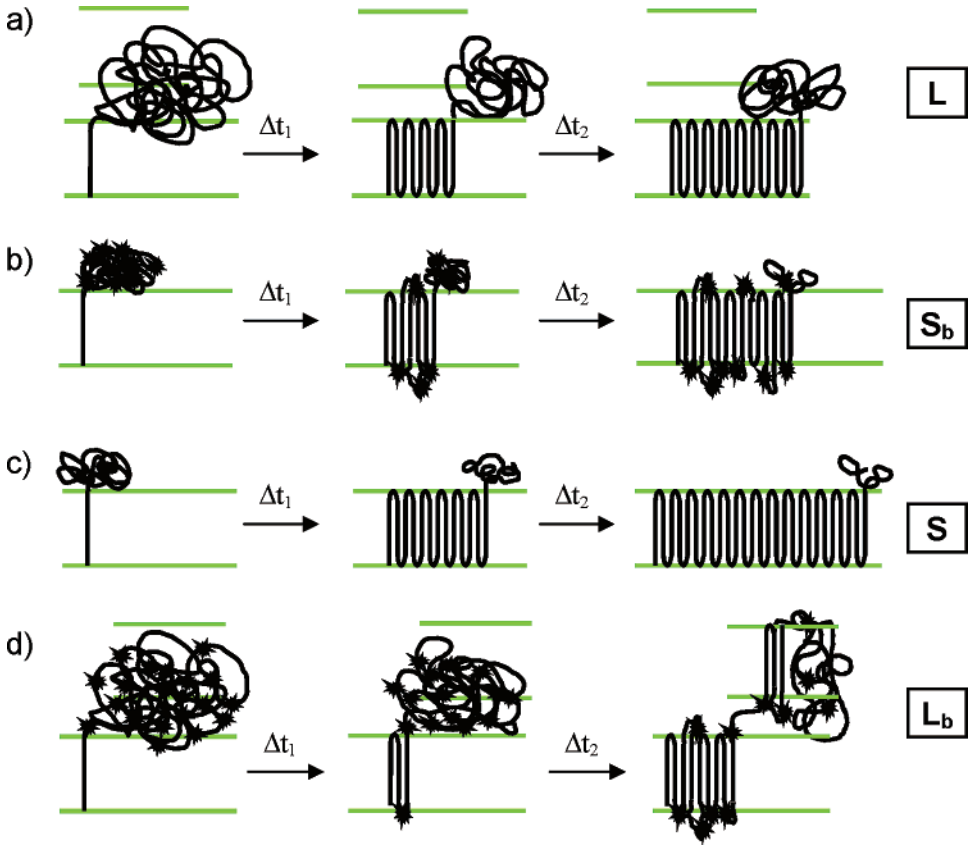

Figure 13. Schematic model depicting crystallization: (a) linear long chain L, (b) branched short chain S_b, (c) linear short chain S, and (d) branched long chain L_b. Parts a and b correspond to the components of the L/S_b blend, while parts c and d correspond to the L_b/S blend. Chain reentry is drawn as adjacent for clarity, but it is understood that there will be nonadjacent reentry as well. The addition of a chain to the growth front will be fastest for S and slowest for L_b. R_g of S and S_b is smaller than the interlamellar spacing so they are unlikely to form interlamellar connections. L and L_b are able to form ties, but as shown, this tendency is exacerbated by the presence of short chain branches in L_b. Details on these effects of length and of presence or absence of SCBs are explained in the text.

Table 3. PENT Failure Times for the Different Binary Blends

blend ID	PENT (h)
L/S_b-52/48	0.1
L/S_b-60/40	0.3
L/S_b-68/32	0.7
L_b/S-52/48	6100
L_b/S-60/40	>12000
L_b/S-68/32	>12000
L′/S_b−52/48	0.5
L′/S_b−60/40	1.1

increases PENT failure time 7-fold (from roughly 6 min to 40 min); and comparing L/S_b blends to their counterparts in the L′/S_b series shows that increasing the length of the long chains confers an additional 4- to 5-fold improvement (extending PENT failure time to just over an hour). Indeed, comparison of blends L_b/S-52/48 and L/S_b-52/48 (with nearly matched M_w, SCB content, ρ, E, σ_y, and ϵ_y) show that the PENT failure time is increased by almost 5 orders of magnitude by placing SCB preferentially on the long chains. Thus, the effect of SCB placement is much stronger than the effect of molecular weight. Furthermore, the PENT failure time improves with increasing long chain content in the L_b/S series—the failure time exceeded 12 000 h (500 days), at which point the test was discontinued. These observations clearly confirm the tremendous importance of branch placement on the long-term fracture behavior of HDPE, with preferential placement of SCB along the longer molecules showing dramatically superior performance.

Discussion

Here we present a conceptual model to rationalize the observed effects of SCB distribution. Placement of SCB on the longer chains in an overall distribution (L_b/S) produces the following changes with respect to an analogous material (similar M_w, MWD and average SCB content) bearing SCBs on the shorter chains (L/S_b): (1) mechanical properties are enhanced (attributed to an increase in interlamellar tie chains). (2) crystallization kinetics are more sluggish at the higher T_x's, but converge as T_x decreases. (3) lamellae formed at the higher T_x's are somewhat thinner (lower T_m), but become similar at the lower T_x's.

Model Assumptions. In the model, as in the present polymers, SCBs are randomly distributed along the chains. The SCB are treated as generic (so it does not account for different comonomer types). It is assumed that the presence of sparse SCBs (∼5 branches/1000 BC) does not significantly change the radius of gyration R_g. For a given overall SCB content, we assume that the equilibrium melting points of the two blends are the same (at infinitely slow crystallization rate, kinetic effects due to the length of the chains bearing the SCBs should vanish). Therefore, for a given crystallization temperature, the undercooling is the same for blends of matched overall SCB content, regardless of whether they are placed on the long or short chains. Finally, our model assumes that only small departures from complete cocrystallization occur in the blends investigated. Mixtures of linear and branched polyethylenes are homogeneous in the melt for all compositions when the branch content is low

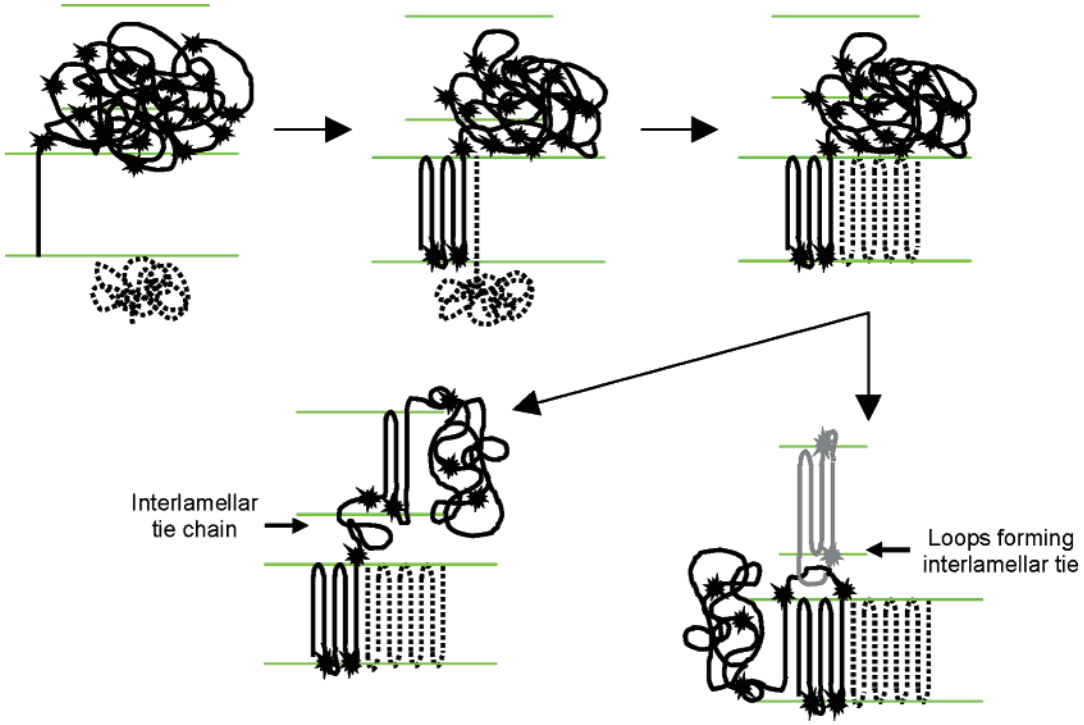

Figure 14. Schematic model of crystallization of the blend L_b/S (short chain branches on the long component) highlighting the interaction between the two species. It depicts how "easier" crystallization of the linear short chain can increase the amount of interlamellar connections. Two types of the latter are shown: one formed by a single tie chain, and another formed by two loops of different chains in adjacent lamellae.

(<40 SCB/1000 BC).[79,80] The model focuses solely on the "growth step" of crystallization because our observations indicated that there were no significant differences in nucleation density.

We consider first the effect of chain length and presence or absence of SCB on the inherent topological and kinetic tendencies of each of the four types of chains that make up our blends (L, S_b, S, and L_b). Subsequently, we take into account the interaction between pairs of linear and SCB chains during crystallization to explain the experimental data regarding final morphology (and mechanical properties) and kinetics of crystallization. In our comparison with experimental results we will frequently refer to the pair of blends L_b/S-52/48 and L/S_b-52/48 (which have similar M_w, MWD, and overall SCB content) as L_b/S and L/S_b respectively.

Molecular Weight Influence. The probability that different segments of a given chain are incorporated into separate lamellae forming ties depends on the length scale spanned by the chain in the melt relative to the interlamellar distance.[81−84] Assuming an interlamellar spacing of about 10 nm and a lamellar thickness of about 25 nm, it is reasonable to conclude that the long chains (L and L_b; $R_g \sim 26$ nm) are much more likely to form interlamellar bridges relative to the short chains (S and S_b; $R_g \sim 8$ nm).

The kinetics of addition of an entangled polymer on a lamellar growth front are affected by the length of the chain due to its strong effect on the conformational relaxation time of the chain. A simple way to envision this effect is to view the growth front as "reeling in" the chain from the melt.[81,82] The rate that segments can be delivered to the substrate is limited by chain transport, which depends on the M_w and T_x.[82] Because long chains have an increased propensity to incorporate within multiple lamellae forming bridges, the lamellar growth kinetics are further impeded.

SCB Influence. Branches bulkier than methyl groups (such as our butyl branches) cannot be incorporated into the polyethylene crystal lattice and, thus, must be rejected.[85] Furthermore, the random placement of SCBs along the backbone will produce a distribution of lengths of crystallizable sequences (i.e., linear stretches between consecutive SCBs).[86] At each T_x there is a "critical sequence length": sequences that are too short will not be adequately undercooled and, therefore, will not crystallize. Thus, it is known that the presence of SCBs on a given polymer chain interferes with its incorporation into a growing lamella. As attachment of segments of a given chain progresses laterally across the face of a growing lamella, a segment bearing a side chain will occasionally be delivered to the growth front. A delay in further addition of that chain will result as the branch or a whole sequence between two branches (if it is not long enough to crystallize at the given T_x) must be excluded and diffuse out of the growth front before crystallization can continue. As a result, the presence of SCBs makes the kinetics of crystallization of L_b and S_b much more sluggish than for L and S, respectively (Figure 13 part d vs a and part b vs c). Furthermore, literature measurements indicate that the presence of SCBs has a much stronger influence than M_w, suggesting that the rate of addition of S_b to a substrate is somewhat slower than that of L chains.

First, we compare the long chains L and L_b. In the case of L (Figure 13 a), its folding back and forth as it adds to the growth front is not interrupted by SCBs. Consequently, the addition to the growth front of L is expected to be fast compared to L_b, and such smooth addition to a given lamella reduces the time during which attachment to another lamella can occur. On the other hand, the presence of SCBs on the L_b chain (Figure 13d) greatly slows addition to the growth front, which affords longer time intervals for other segments of the L_b chain to attach to other lamellae (forming tie chains) or to separate locations on the same lamella (forming loops that can interlock and thereby link separate lamellae). Thus, L_b has greater tendency than L to form interlamellar ties. The scenario changes when we consider the effect of SCBs on the short molecules: although

the crystallization kinetics of S_b (Figure 13 b) are disrupted relative to those of S, its relatively low R_g will make it unlikely to form interlamellar connections. Consequently, the topological consequences of SCBs depend on whether they are placed on the short or long chains in an overall distribution: L_b tends to form tie chains to a much greater extent than any of the other three species.

L/S$_b$ Blend vs L$_b$/S Blend. In addition to the inherent molecular characteristics for each individual component, interactions between the pair of polymers in each blend contribute to the qualitative differences between L/S_b (Figure 13, parts a and b) and L_b/S blends (Figure 13, parts c and d).

Tie Chains. First we consider crystallization in a L_b/S blend. The S component has the lowest tendency of all to form tie chains, but the L_b component has the highest. In this blend, such predisposition of L_b is exacerbated by the interaction of both components as schematically depicted in Figure 14. The kinetic trapping of L_b segments in crystals due to the rapid addition of S chains around them further increases the propensity of L_b to form tie chains: L_b chains experience topological frustrations when they compete with S chains that are able to crystallize much faster, rapidly occupying nearby sites on the growth front. This obliges the dangling portion of the L_b chain to deposit somewhere else, either on the same lamella forming loops or on a nearby lamella forming tie chains. Thus, the interactions between the species in the binary blend increase the propensity of L_b/S to form tie chains and, consequently, enhances mechanical properties. On the contrary, the components of the L/S_b blend do not have radically different velocities at which they deposit and reel in onto the growth front. Adding SCB slows addition to the growth front as does increasing chain length. Given that the effect of SCB is stronger, it is possible that L chains could "pin" S_b chains onto the growth front. However, even if some S_b chains were kinetically trapped by faster adding L chains, their small R_g would make it unlikely for them to form interlamellar links.

Regarding the differences observed at high T_x, we first consider the L/S_b blend. Using literature growth front velocities G,[82,87−90] we estimate that at 124 °C, a unimodal melt of L would have $G \leq 0.02$ μm/s, while for a melt of S_b, $G \sim 0.006$ μm/s.[91] Thus, 0.02 μm/s provides an upper bound for the linear growth rate in the blend L/S_b. Also, literature values [92−94] may be used to estimate that a S_b molecule can diffuse $\sim$1 μm in $\sim$1 s in a monomodal melt.[95] Considering these values, during crystallization of the blend, while some S_b segments will be incorporated into the lamella, the diffusivity of S_b is great enough that many S_b segments may diffuse out of the growth front. Even tethered S_b chains (with at least one segment incorporated into a crystal) will have time for conformational rearrangement that moves their SCBs out of the growth front and preferentially into the adjacent noncrystalline layers.

In contrast, in a L_b/S blend the S chains cause the growth velocity to exceed the rate at which L_b can escape. On the basis of literature values, a melt of S would have G(124 °C) $\sim$ 0.2 μm/s, orders of magnitude greater than a melt of L_b, which would have $G \sim 0.0005$ μm/s.[82,87−91] Thus, G of the blend is expected to be between these two values. Diffusion of L_b chains only allows them to translate at $\sim$0.0007 μm/s.[92−96] Therefore, the L_b chains cannot escape; instead, they must participate in crystallization and optimize their addition to the growth front to the extent permitted by kinetic constraints. Relative to the L/S_b blend, more SCB strands (of L_b) are incorporated into the growing lamellae in L_b/S. As a result, even with the same average chain lengths and average SCB content, there will be an overall slowing down of the kinetics of crystallization in L_b/S relative to L/S_b (as observed by DSC). The kinetic trapping of a greater number of SCB chain segments in the lamellae can also explain more imperfect lamellae and lower melting points for L_b/S vs L/S_b.

Regarding the disappearance of differences as T_x decreases, we note that G becomes so fast ($\sim$ 0.2 μm/s at 119 °C) that even the short chains S_b cannot escape the growth front in L/S_b. In contrast, the physical picture for the L_b/S blend is not changed by decreasing T_x, since the L_b chains are already unable to "keep up" with propagation of the growth front at any T_x examined. Therefore, the crystallization behaviors of the two blends converge with decreasing T_x, as it is observed in the overall kinetics and melting temperatures as T_x decreases from 124 to 119 °C. Note that the arguments for increased tie chain formation in L_b/S hold at all T_x examined.

Conclusions

The crystallization kinetics and topology−hence the ultimate morphology and performance−of PE products depend on the distribution of branches along the MWD of the polymer in addition to molecular weight, MWD, and total SCB content. While many previously published reports discuss the influences exerted by molecular weight, crystallinity, and SCB content on the properties of PE, to our knowledge this is the first report that examines the influence of branching distribution.

Bimodal Blends Serving as Model Systems. Each component of the blend was well characterized in terms of molecular weight, MWD and SCB. By blending individual components we created materials with known concentration of SCB chains, with known degree of branching and known chain length. The two components in each blend differed by approximately 10-fold in molecular weight, with SCBs placed exclusively on either the "short" ($\sim$ 40 kg/mol) or the "long" (400 kg/mol and 550 kg/mol) chains.

Crystallization kinetics experiments indicate much slower lamellar growth rates, particularly at high temperatures, for blends with preferential placement of SCB on the longer chains. The mechanical properties of the binary blends clearly show that placing SCBs on the long chains produces considerably superior performance (ultimate tensile failure, slow crack growth fracture, and impact fracture) relative to materials having similar M_w, MWD and average SCB content, but with SCBs on the short chains. This macroscopic observation suggests that placing SCBs on the long chains favors the formation of interlamellar tie chains.

We developed a conceptual model that explains this enhancement of tie chain formation, as well as the trends in crystallization kinetics and lamellar thickness, due to SCBs on the long chains rather than the short chains. The model suggests that inherent crystallization tendencies of individual components, as well as kinetic interactions between competing species at the growth front combine to cause the observed macroscopic consequences of SCB distribution.

This work on PE should also provide a framework for molecular design of other semicrystalline polymers that allow for the introduction of noncrystallizable defects along the polymer backbone. This investigation has tremendous practical implications because many commercial PE resins are produced either by blending reactor product from series or parallel reactors or by blending polymers with and without SCB to tailor product performance.

Acknowledgment. The authors would like to acknowledge useful discussions with Prof. Stephen Cheng (University of

Akron) and Prof. Garth Wilkes (Virginia Tech). Dr. Paul DesLauriers and Dr. David Rohlfing are acknowledged for molecular weight and rheological characterization of the polymers and blends. The authors are also grateful to Barbara Lewis, Jim French, Jerry Stark, David Higbee, Tim Harper, and Delores Henson for performing most of the experiments. Financial support by the National Science Foundation (Grants DMI-0218112 and DMI-0523083) is acknowledged.

References and Notes

(1) Peacock, A. J. *Handbook of Polyethylene: Structure, Properties and Applications*; Marcel Dekker: New York, 2000.
(2) Lustiger, A.; Markham, R. L. *Polymer* **1983**, *24*, 1647.
(3) Lu, X.; Zhou, Z.; Brown, N. *Polym. Eng. Sci.* **1997**, *37*, 1896.
(4) Bailey, F. W.; Whitte, W. M. United States Patent 4,461,873, 1984; United States Patent 4,547,551, 1985.
(5) Nishimura, H.; Maeba, H. *Proceedings of the 10th International Plastics Pipes Conference*; Goteborg, Sweden, 1998.
(6) Mandelkern, L. *Polym. J.* **1985**, *17*, 337.
(7) Brady, J. M.; Thomas, E. L. *J. Polym. Sci., Polym. Phys. Ed.* **1988**, *26*, 2385.
(8) Alamo, R. G.; Mandelkern, L. *Macromolecules* **1989**, *22*, 1273.
(9) Alamo, R. G.; Mandelkern, L. *Macromolecules* **1991**, *24*, 6480.
(10) Alamo, R. G.; Chan, E. K. M.; Mandelkern, L.; Voight-Martin, I. G. *Macromolecules* **1992**, *25*, 6381.
(11) Kennedy, M. A.; Peacock, A. J.; Failla, M. D.; Lucas, J. C.; Mandelkern, L. *Macromolecules* **1995**, *28*, 1407.
(12) Wignall, G. D.; Alamo, R. G.; Londono, J. D.; Mandelkern, L.; Kim, M. H.; Lin, J. S.; Brown, G. M. *Macromolecules* **2000**, *33*, 551.
(13) Haigh, J. A.; Nguyen, C.; Alamo, R. G.; Mandelkern, L. *J. Therm. Anal. Calorim.* **2000**, *59*, 435.
(14) Crist, B.; Howard, P. R. *Macromolecules* **1999**, *32*, 3057.
(15) Crist, B.; Claudio, E. S. *Macromolecules* **1999**, *32*, 8945.
(16) Alizadeh, A.; Richardson, L.; Xu, J.; McCartney, S.; Marand, H.; Cheung, Y. W.; Chum, S. *Macromolecules* **1999**, *32*, 6221.
(17) Mirabella, F. M. *J. Polym. Sci., Polym. Phys. Ed.* **2001**, *39*, 2800.
(18) Kim, J. −H.; Phillips, P. J. *J. Appl. Polym. Sci.* **1998**, *70*, 1893.
(19) Wagner, J.; Abu-Iqyas, S.; Monar, K.; Phillips, P. J. *Polymer* **1999**, *40*, 4717.
(20) Fu, Q.; Chiu, F−C.; McCreight, K. W.; Guo, M.; Tseng, W. W.; Cheng, S. Z. D.; Keating, M. Y.; Hsieh, E. T.; DesLauriers, P. J. *J. Macromol. Sci., Phys. Ed.* **1997**, *B36*, 41.
(21) Vanden Eynde, S.; Mathot, V.; Koch, M. H. J.; Reynaers, H. *Polymer* **2000**, *41*, 3437.
(22) Akpalu, Y.; Kielhorn, L.; Hsiao, B. S.; Stein, R. S.; Russell, T. P.; van Egmond, J.; Muthukumar, M. *Macromolecules* **1999**, *32*, 765.
(23) Janimak, J. J.; Bassett, D. C. *Polymer* **1999**, *40*, 459.
(24) Hosier, I. L.; Bassett, D. C. *Polym. J.* **1999**, *31*, 772.
(25) Jordens, K.; Wilkes, G. L.; Janzen, J.; Rohlfing, D. C.; Welch, M. B. *Polymer* **2000**, *41*, 7175.
(26) Janzen, J.; Register, D. F. *Proc. SPE ANTEC* **1996**, *2*, 2190.
(27) Janzen, J. *Polym. Eng. Sci.* **1992**, *32*, 1242.
(28) Janzen, J. *Polym. Eng. Sci.* **1992**, *32*, 1255.
(29) Crist, B.; Fisher, C. J.; Howard, P. R. *Macromolecules* **1989**, *22*, 1709.
(30) Popli, R.; Mandelkern, L. *J. Polym. Sci., Polym. Phys. Ed.* **1987**, *25*, 441.
(31) Peacock, A. J.; Mandelkern, L. *J. Polym. Sci., Polym. Phys. Ed.* **1990**, *28*, 1917.
(32) Failla, M. D.; Lucas, J. C.; Mandelkern, L. *Macromolecules* **1994**, *27*, 1334.
(33) Kennedy, M. A.; Peacock, A. J.; Mandelkern, L. *Macromolecules* **1994**, *27*, 5297.
(34) Peacock, A. J.; Mandelkern, L.; Alamo, R. G.; Fatou, J. G. *J. Mater. Sci.* **1998**, *33*, 2255.
(35) Brown, N.; Ward, I. M. *J. Mater. Sci.* **1983**, *18*, 1405.
(36) Brooks, N. W.; Ghazali, M.; Duckett, R. A.; Unwin, A. P.; Ward, I. M. *Polymer* **1999**, *40*, 821.
(37) Hill, R. *J. Mech. Phys. Solids* **1965**, *13*, 213.
(38) Budiansky, B. *J. Mech. Phys. Solids* **1965**, *13*, 223.
(39) Williams, J. G. *Fracture Mechanics of Polymers*; Ellis Horwood: West Sussex, England, 1987.
(40) Ward, I. M.; Sweeney, J. *An Introduction to the Mechanical Properties of Solid Polymers*; John Wiley and Sons: West Sussex, England, 2004.
(41) Brown, N.; Bhatacharya, S. K. *J. Mater. Sci.* **1985**, *20*, 4553.
(42) Lu, X.; Brown, N. *Polymer*, **1987**, *28*, 1505.
(43) Wang, X.; Brown, N. *Polymer* **1988**, *29*, 463.
(44) Lu, X.; Wang, Z.; Brown, N. *J. Mater. Sci.* **1988**, *23*, 643.
(45) Wang, X.; Brown, N. *Polymer* **1989**, *30*, 1456.
(46) Lu, X.; Brown, N. *J. Mater. Sci.* **1990**, *25*, 411.
(47) Lu, X.; Qian, R.; Brown, N. *J. Mater. Sci.* **1991**, *26*, 917.
(48) Ward, A. L.; Lu, X.; Brown, N. *Polym. Eng. Sci.* **1990**, *30*, 1175.
(49) Huang, Y. L.; Brown, N. *J. Polym. Sci., Polym. Phys. Ed.* **1990**, *28*, 2007.
(50) Huang, Y. L.; Brown, N. *J. Polym. Sci., Polym. Phys. Ed.* **1991**, *29*, 129.
(51) Huang, Y. L.; Brown, N. *Polymer* **1992**, *33*, 2989.
(52) Hubert, L.; David, L.; Sequela, R.; Vigier, G.; Degoulet, C.; Germain, Y. *Polymer* **2001**, *42*, 8425.
(53) Hubert, L.; David, L.; Sequela, R.; Vigier, G.; Corfias-Zuccalli, C.; Germain, Y. *J. Appl. Polym. Sci.* **2002**, *84*, 2308.
(54) Lustiger, A.; Ishikawa, N. *J. Polym. Sci., Polym. Phys. Ed.* **1991**, *29*, 1047.
(55) Krishnaswamy, R. K. *Polymer* **2005**, *46*, 11664.
(56) Krishnaswamy, R. K. *Polym. Eng. Sci.*, in press.
(57) Hsieh, E. T.; Tso, C. C.; Byers, J. D.; Johnson, T. W.; Fu, Q.; Cheng, S. Z. D. *J. Macromol. Sci., Phys. Ed.* **1997**, *B36*, 615.
(58) DesLauriers, P. J.; Rohlfing, D. C.; Hsieh, E. T. *Polymer* **2002**, *43*, 159.
(59) Rohlfing, D. C.; Janzen, J. Melt rheological characterization of metallocene-catalyzed polyethylenes. In *Metallocene-Based Polyolefins*; Scheirs, J., Kaminsky, W., Eds.; John Wiley & Sons: New York, 2000; p 419.
(60) Janzen, J.; Colby, R. H. *J. Mol. Struct.* **1999**, *569*, 485−486.
(61) Krishnaswamy, R. K.; Janzen, J. *Polym. Test.* **2005**, *24*, 762.
(62) DiLorenzo, M. L.; Silvestre, C. *Prog. Polym. Sci.* **1999**, *24*, 917.
(63) Nadkarni, V. M.; Bulakh, N. N.; Jog, J. P. *Adv. Polym. Technol.* **1993**, *12*, 73.
(64) Ozawa, T. *Polymer* **1971**, *12*, 150.
(65) McCrum, N. G.; Read, B. E.; Williams, G. *Anelastic and Dielectric Effects in Polymeric Solids*; Dover Publications: New York 1991 (John Wiley and Sons: New York, 1967).
(66) Boyd, R. H. *Polymer* **1985**, *26*, 323.
(67) Boyd, R. H. *Polymer* **1985**, *26*, 1123.
(68) Popli, R.; Glotin, M.; Mandelkern, L. *J. Polym. Sci., Polym. Phys. Ed.* **1984**, *22*, 407.
(69) Khanna, Y. P.; Turi, E. A.; Taylor, T. J.; Vickroy, V. V.; Abbot, R. F. *Macromolecules* **1985**, *18*, 1302.
(70) Mathews, R. G.; Unwin, A. P.; Ward, I. M.; Capaccio, G. *J. Macromol. Sci., Phys. Ed.* **1999**, *B38*, 123.
(71) Hiss, R.; Hobeika, S.; Lynn, C.; Strobl, G. *Macromolecules* **1999**, *32*, 4390.
(72) Bartczak, Z. *Macromolecules* **2005**, *38*, 7702.
(73) Bartczak, Z.; Lezak, E. *Polymer* **2005**, *46*, 6050.
(74) Kurelac, L.; Teeuwen, M.; Schoffeleers, H.; Deblieck, R. *Polymer* **2005**, *46*, 6369.
(75) Bartczak, Z.; Kozanecki, M. *Polymer* **2005**, *46*, 8210.
(76) Bartczak, Z. *Polymer* **2005**, *46*, 10339.
(77) Brown, N.; Lu, X. *Polym. Eng. Sci.* **2001**, *41*, 1140.
(78) Krishnaswamy, R. K.; Leevers, P. S.; Lamborn, M. J.; Sukhadia, A. M.; Register, D. F.; Maeger, P. L. *Polym. Eng. Sci.* **2006**, *46*, 1358.
(79) Alamo, R. K.; Graessley, W. W.; Krishnamoorti, R.; Lohse, D. J.; Londono, J. D.; Mandelkern, L.; Stehling, F. C.; Wignall, G. D. *Macromolecules* **1997**, *30*, 561.
(80) Galante, M. J.; Mandelkern, L.; Alamo, R. G. *Polymer* **1998**, *39*, 5105.
(81) Hoffman, J. D.; Miller, R. L. *Macromolecules* **1988**, 3038.
(82) Hoffman, J. D.; Miller, R. L. *Polymer* **1997**, 3151.
(83) Sperling, L. H. *Introduction to Physical Polymer Science*; Wiley-Interscience: New York, 2001.
(84) Schultz, J. M. *Polymer Crystallization*; Oxford University Press: Washington, DC, 2001.
(85) Alamo, R.; Domszy, R.; Mandelkern, L. *J. Phys. Chem.* **1984**, *88*, 6587.
(86) Flory, P. J. *Trans Faraday Soc.* **1955**, *51*, 848.
(87) Wagner, J.; Abu-Iqyas, S.; Monar, K.; Philips, P. J. *Polymer* **1999**, *40*, 4717.
(88) Wagner, J.; Phillips, P. J. *Polymer* **2001**, *42*, 8999.
(89) Hoffman, J. D.; Frolen, L. J.; Gaylon, S. R.; Lauritzen, J. I. *J. Res. Natl. Bur. Stand. A: Phys. Chem.* **1975**, *79A*, 671.
(90) Armistead, J. P.; Hoffman, J. D. *Macromolecules* **2002**, *35*, 3895.
(91) Linear growth velocity, G, was estimated from literature values. For S we interpolated between G for linear 31K[52] and 75K.[59,60] For L we extrapolated from G for linear PE of 100K, 210K, and 266K.[57−59] The effects of SCB on G are much stronger than those of M_w. Therefore, G of S_b was estimated to be very similar to a 60K PE with ∼ 4 SCB/1000 BC (57, 58). Finally, G for L_b was extrapolated from the dependence of linear growth rate with M_w for copolymers of similar short chain branching (60K with 4 SCB/1000 BC and 117K with 5.5 SCB/1000 BC, refs 87 and 88). The temperature dependence of G was used for estimations when data was available close to but not exactly at the temperature of interest. The estimated values are approximate; however, their order of magnitude is such that small variations would not change our discussion.

(92) Pearson, D. S.; Ver Strate, G.; von Meerwall, E.; Schilling, F. C. *Macromolecules* **1987**, *20*, 1133.
(93) Pearson, D. S.; Fetters, L. J.; Graessley, W. W.; Ver Strate, G.; von Meerwall, E. *Macromolecules* **1994**, *27*, 711.
(94) Bartels, C. R.; Crist, B.; Graessley, W. W. *Macromolecules* **1984**, *17*, 2702.
(95) Although literature values for HDPE are sparse and refer to samples with a certain degree of polydispersity,[92] values for the diffusivity of (model) hydrogenated polybutadienes are available at 175°C as a function of molecular weight.[93,94] The temperature dependence has been described to fit well with an Arrhenius type expression with activation energy of 26 kJ/mol, allowing calculation of diffusivity at 125°C. Also, note that in a blend, the diffusivity of short molecules is negligibly affected by the presence of the long molecules (since they tend to reduce any constraint release that may have been operative in the unimodal case). For the L chain lengths used here, the diffusivity of the long chains also retains the value that it has in a unimodal melt despite the presence of the short chains: the ratio of molecular weights is such that it is known that constraint release does not dominate the diffusion of the long chains.[96.]
(96) Rubinstein, M.; Colby, R. H. *Polymer Physics*; Oxford University Press: New York, 2003.

MA070454H